Planet. Space Sci. 1970, Vol. 18, pp. 271 to 285. Pergamon Press. Printed in Northern Ireland

ATOMIC OXYGEN INFRARED EMISSION IN THE EARTH'S UPPER ATMOSPHERE

G. KOCKARTS and W. PEETERMANS
Institut d'Aéronomie Spatiale de Belgique, 3, Avenue Circulaire, Bruxelles 18, Belgium

(*Received* 1 *September* 1969)

Abstract—The atomic oxygen emission at 63 μ is analyzed between 50 km and 250 km for several atmospheric models. The frequency integrated intensities and the volume emission rates are computed and discussed in connection with experimental and theoretical investigations of the atomic oxygen distribution. It is shown that radiative transfer should be used below 150 km. If an infrared emission occurs near the tropopause, the radiative transfer solutions leads to an infrared heating near the mesopause. A reduction factor is introduced for comparison with an optically thin atmosphere.

1. INTRODUCTION

The main heat input in the thermosphere results from the absorption of solar ultraviolet radiation by atmospheric constituents, and the heat thereby deposited is transported downwards by conduction. However, a complete study of the heat transport phenomena requires a knowledge of the production and loss terms. Among the atmospheric components present above 100 km altitude, atomic oxygen is able to emit in the far infrared and in this way may play a role in the thermal balance of the thermosphere.

The importance of an infrared loss at 63 μ due to the transition $O(^3P_1) \rightarrow O(^3P_2)$ was first demonstrated by Bates (1951) in his determination of the rate of energy loss in an optically thin atmosphere. Münch (1962), in a study of the problem of the intensity of forbidden emission lines, applied his results to the atomic oxygen emission at 63 μ. In his work he questioned whether this emission is measurable and concluded that "such an experiment offers a challenge to infrared technology, but, when carried out, it will provide very valuable data about the structure of the upper atmosphere." Such an experiment has just been carried out by Feldman and McNutt (1969) and by Houck and Harwit (1969). Even if, as stated by the authors (Feldman and McNutt, 1969), the data reported are far from ideal, these first observational results will be discussed here.

After adopting working models of the atmosphere and determining the infrared loss without radiative transfer, the optical depth involved in the computations and the radiative transfer equation are discussed. The numerical results for the intensity and the flux and the volume emission rate of the 63 μ line are obtained, and the effect of a change in the atomic oxygen concentration is also described.

2. INFRARED LOSS IN AN OPTICALLY THIN ATMOSPHERE

The infrared energy of atomic oxygen is emitted through magnetic dipole transitions (see Fig. 1). Numerical values taken from tables prepared by Wiese *et al.* (1966) show the rather high transition probabilities involved and the low excitation potentials of the transitions $^3P_0 - {}^3P_1$ at 147 μ and $^3P_1 - {}^3P_2$ at 63 μ, respectively.

If we assume a Boltzmann distribution, the ratio of the oxygen concentration n_J in the state ^3P_J to the total atomic oxygen concentration $n(O)$ is given by the relation:

$$n_J/n(O) = \frac{g_J \exp(-E_J/kT)}{\sum_J g_J \exp(-E_J/kT)} \quad (1)$$

where g_J is the statistical weight $2J + 1$ of the level J, E_J the energy above the ground level, k the Boltzmann constant and T the kinetic temperature. The hypothesis of a Boltzmann distribution has been discussed by Bates (1951) and in detail by Münch (1962). In what follows, the identifying subscripts 0, 1 and 2 refer to the quantum number J of the triplet ground state of atomic oxygen, unless specifically mentioned otherwise.

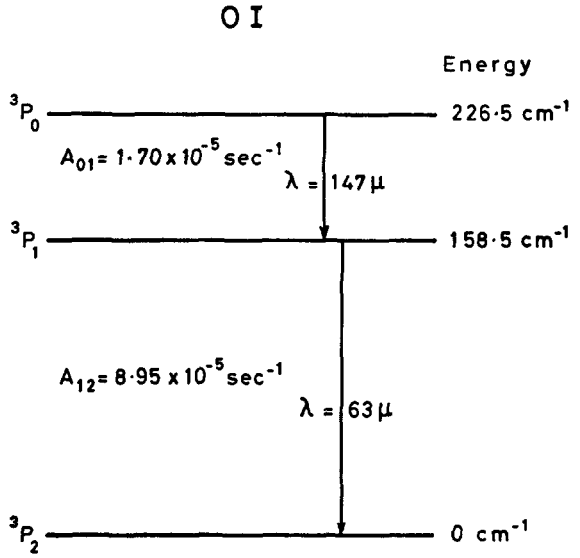

FIG. 1. ATOMIC OXYGEN GROUND STATE TRANSITIONS.

In order to determine the atomic oxygen infrared emission, models of the atomic oxygen vertical distribution must be adopted. Figure 2 shows the vertical distributions between 50 km and 300 km altitude with two extreme profiles above 120 km which correspond to thermopause temperatures of 750 and 2000°K (Table 1).

Below 80 km, two distributions corresponding to daytime and night-time conditions in the mesosphere are also considered (Table 2).

The daytime curve corresponds approximately to a photoequilibrium distribution for an overhead Sun (Nicolet *et al.*, 1970). The atomic oxygen concentration is not yet sufficiently known, and there is probably a great variability in the region around 120 km. At this altitude we have adopted a value of 10^{11} cm^{-3}, whereas mass spectrometric measurements (Krankowsky *et al.*, 1968) give values as low as 10^{10} cm^{-3}. Other measurements (Mauersberger *et al.*, 1968), however, correspond to a concentration of $5{\cdot}7 \times 10^{10}$ cm^{-3}. The highest experimental values known at this time are those obtained by Hall *et al.* (1967) and by Hinteregger and Hall (1969). From ultraviolet absorption measurements (Hinteregger and Hall, 1969), the atomic oxygen concentration at 350 km altitude is in the range from $3{\cdot}1 \times 10^8$ cm^{-3} at sunrise to $5{\cdot}5 \times 10^8$ cm^{-3} at sunset for a thermopause temperature of 1000°K. In the working model corresponding to the same thermopause temperature the atomic oxygen concentration has a value of $2{\cdot}6 \times 10^8$ cm^{-3} at 350 km. Without entering into a detailed discussion, it can be said that the variations of the atomic oxygen distribution are due not only to temperature changes but also to the hydrodynamical regime above the mesopause. The vertical distribution depends in fact strongly on the eddy

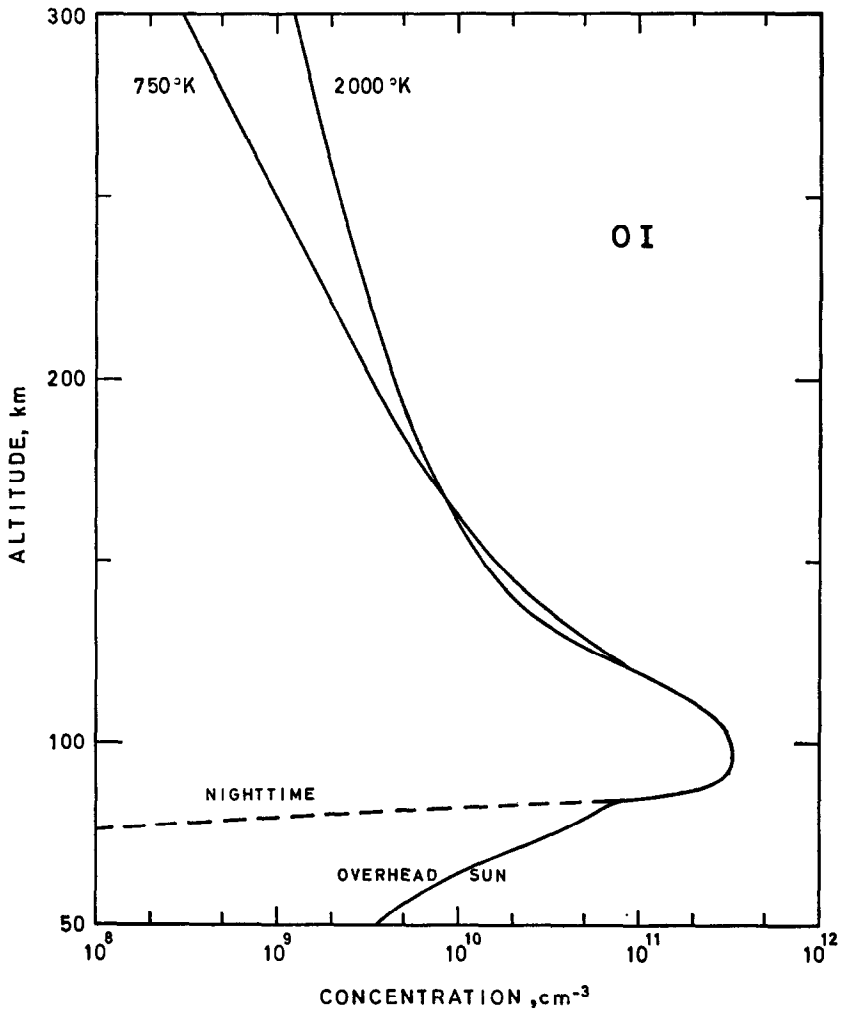

FIG. 2. VERTICAL DISTRIBUTION OF ATOMIC OXYGEN CONCENTRATIONS FOR THERMOPAUSE TEMPERATURES OF 750 AND 2000°K.
Mesospheric and lower thermospheric distributions for nighttime and overhead Sun conditions.

TABLE 1. ATOMIC OXYGEN CONCENTRATION (cm^{-3}) IN THE THERMOSPHERE

z (km)	120	150	200	250	300
$T = 750°K$	$1{\cdot}00 \times 10^{11}$	$1{\cdot}67 \times 10^{10}$	$3{\cdot}67 \times 10^{9}$	$1{\cdot}01 \times 10^{9}$	$3{\cdot}12 \times 10^{8}$
$T = 2000°K$	$1{\cdot}00 \times 10^{11}$	$1{\cdot}38 \times 10^{10}$	$4{\cdot}45 \times 10^{9}$	$2{\cdot}25 \times 10^{9}$	$1{\cdot}31 \times 10^{9}$

diffusion coefficients (Colegrove *et al.*, 1966) which are poorly known in the lower thermosphere.

Without any reabsorption, the infrared emissions L at 63 μ and at 147 μ can be written respectively as:

$$L(63\ \mu) = (E_1 - E_2)A_{12}n_1 \tag{2}$$

and

$$L(147\ \mu) = (E_0 - E_1)A_{01}n_0 \tag{3}$$

TABLE 2. ATOMIC OXYGEN CONCENTRATION (cm^{-3}) IN THE MESOSPHERE AND IN THE LOWER THERMOSPHERE

z (km)	50	60	70	80	90	100	110
Overhead Sun	$3{\cdot}5 \times 10^{9}$	$6{\cdot}9 \times 10^{9}$	$2{\cdot}0 \times 10^{10}$	$5{\cdot}4 \times 10^{10}$	$3{\cdot}0 \times 10^{11}$	$3{\cdot}2 \times 10^{11}$	$2{\cdot}3 \times 10^{11}$
night-time	—	—	$9{\cdot}0 \times 10^{5}$	$2{\cdot}2 \times 10^{9}$	$3{\cdot}0 \times 10^{11}$	$3{\cdot}2 \times 10^{11}$	$2{\cdot}3 \times 10^{11}$

where A_{12} and A_{01} are the transition probabilities given in Fig. 1. By using Equation (1), the energy losses (2) and (3) are written as follows:

$$L(63\mu) = \frac{1{\cdot}69 \times 10^{-18} n(\mathrm{O}) \exp(-228/T)}{1 + 0{\cdot}6 \exp(-228/T) + 0{\cdot}2 \exp(-326/T)} \tag{4}$$

and

$$L(147\ \mu) = \frac{4{\cdot}59 \times 10^{-20} n(\mathrm{O}) \exp(-326/T)}{1 + 0{\cdot}6 \exp(-228/T) + 0{\cdot}2 \exp(-326/T)} \tag{5}$$

in units of erg cm^{-3} sec^{-1}.

Table 3 gives the energy rate R (erg sec^{-1}) emitted for temperatures ranging from 200 to 2000°K. The energy rate at 147 μ is less than 3 per cent of the energy rate at 63 μ, even

TABLE 3. ENERGY RATE (erg sec^{-1}) EMITTED AT 63 μ AND AT 147 μ

T (°K)	200	300	400	500	600	700	800	900	1000	1500	2000
$R(63\ \mu) \times 10^{19}$	4·36	5·83	6·65	7·17	7·53	7·78	7·97	8·13	8·25	8·61	8·79
$R(147\ \mu) \times 10^{20}$	0·73	1·15	1·42	1·61	1·75	1·85	1·93	1·99	2·04	2·20	2·29

for a temperature of 2000°K. We consider therefore only the emission at 63 μ, although the following mathematical formulation is identical for the emission at 147 μ.

3. RADIATIVE TRANSFER EQUATION

If we denote by I_ν the *specific intensity* (erg cm^{-2} sec^{-1} $ster.^{-1}$ Hz^{-1}) emitted at frequency ν in the direction s, the radiative transfer equation can be written, according to Chandrasekhar (1960), in the following form:

$$\mathrm{d}I_\nu/\mathrm{d}s = -\kappa_\nu I_\nu + \varepsilon_\nu \tag{6}$$

where κ_ν is an absorption coefficient measured in cm^{-1} and ε_ν is the energy emitted at frequency ν (erg cm^{-3} $ster.^{-1}$ sec^{-1} Hz^{-1}).

If the direction s makes an angle θ with the vertical z measured positively from the Earth's surface ($\mathrm{d}z = \cos\theta\ \mathrm{d}s = u\ \mathrm{d}s$), Equation (6) can be transformed into:

$$u\ \mathrm{d}I_\nu/\mathrm{d}z = -\kappa_\nu I_\nu + \varepsilon_\nu. \tag{7}$$

In the upper atmosphere, it is possible to consider the 63 μ line with a Doppler width $\Delta\nu$ and therefore with the following coefficients:

$$\varepsilon_\nu = \frac{A_{12}(E_1 - E_2) n_1}{4\pi\Delta\nu} \tag{8}$$

and

$$\kappa_\nu = (n_2 B_{21} - n_1 B_{12}) \frac{(E_1 - E_2)}{4\pi\Delta\nu} . \tag{9}$$

The Einstein coefficients A_{12}, B_{21} and B_{12} in (8) and (9) are given by

$$B_{21} = A_{12} \frac{g_1}{g_2} \frac{c^2}{2h\nu^3} \tag{10}$$

and

$$B_{21} = (g_2/g_1) B_{12} \tag{11}$$

where h is Planck's constant, ν the frequency of the radiation and c the speed of light. In Equation (9), the first term represents the absorption by the atoms in the state $^3P_2$, whereas the second term takes into account the stimulated emission which reduces the importance of the absorption process.

By introducing the optical depth derivative $\mathrm{d}\tau/\mathrm{d}z$ defined by

$$\mathrm{d}\tau/\mathrm{d}z = -\kappa_\nu \tag{12}$$

Equation (7) can finally be written, with the help of relations (1) and (8) to (12), in the form

$$u\, \mathrm{d}I_\nu/\mathrm{d}\tau = I_\nu - (2h\nu^3/c^2)[\exp (E_1 - E_2)/kT - 1]^{-1} \tag{13a}$$

or

$$u\, \mathrm{d}I_\nu/\mathrm{d}\tau = I_\nu - B(T) \tag{13b}$$

since $B(T)$ is the specific intensity at frequency ν of a black body characterized by a temperature T, which depends on the altitude, i.e. on the optical depth.

The specific intensity is not easily accessible to experimental determinations. Actually, one measures the *frequency integrated intensity* $I = \int I_\nu \, \mathrm{d}\nu$, or with a certain approximation $I = I_\nu \Delta\nu$. Such a procedure is equivalent to considering a rectangular profile with a width $\Delta\nu$ equal to the Doppler width. The frequency integrated intensities can therefore be obtained by multiplying the solutions of (13b) by $\Delta\nu$. This procedure is not valid in the case of a molecular rotational spectrum for which each line has not necessarily a Doppler shape and for which some lines may partially overlap.

If we neglect absorption and stimulated emission, i.e. if $\kappa_\nu = 0$, Equations (7) and (8) lead to the frequency integrated intensity in the following form

$$4\pi I^* = A_{12}(E_1 - E_2) \int_z^\infty n_1 \sec\theta \, \mathrm{d}z. \tag{14}$$

Along the vertical ($\theta = 0$), such a frequency integrated intensity or apparent emission rate $4\pi I^*$ given in erg cm^{-2} sec^{-1} column^{-1} is identical to the integration of the infrared loss (2). Such an expression has been used by Feldman and McNutt (1969) in the analysis of their data.

4. ABSORPTION CROSS SECTION AND OPTICAL DEPTH

If a Doppler profile is adopted for the infrared line, the absorption cross section $\sigma(\nu)$ as a function of frequency is given by

$$\sigma(\nu) = \sigma(\nu_0) \exp \left[- \frac{2(\nu - \nu_0)}{\Delta\nu} \sqrt{\ln 2} \right]^2 \tag{15}$$

where $\sigma(\nu_0)$ is the cross section at the center of the line at frequency ν_0 (Mitchell and Zemansky, 1961). The total Doppler width is given by

$$\Delta\nu = 2\frac{\nu_0}{c}\left(\frac{2kT\ln 2}{m}\right)^{1/2} = 8{\cdot}51 \times 10^5\, T^{1/2}\,(\mathrm{Hz}) \tag{16}$$

where m is the mass of an oxygen atom.

In expression (9) a weighed cross section $\bar{\sigma}$ is introduced such that

$$\int_0^\infty \sigma(\nu)\,\mathrm{d}\nu = \frac{B_{21}}{4\pi}(E_1 - E_2) = \bar{\sigma}\,\Delta\nu. \tag{17}$$

In his computation, Bates (1951) used the cross section at the center of the line $\sigma(\nu_0)$, which is related to our weighed cross section by

$$\sigma(\nu_0) = 2(\pi/\ln 2)^{1/2}\bar{\sigma} = 0{\cdot}94\bar{\sigma}. \tag{18}$$

For temperature ranging from 200 to 2000°K, $\bar{\sigma}$ varies from $7{\cdot}1 \times 10^{-18}$ cm^2 to $2{\cdot}2 \times 10^{-16}$ cm^2 following a law in $T^{-1/2}$.

Taking into account (1), (9), (10), (11) and (16), the derivative of the optical depth (12) may be written as follows

$$\frac{\mathrm{d}\tau}{\mathrm{d}z} = \frac{-1{\cdot}0 \times 10^{-16}T^{-1/2}n(\mathrm{O})[\exp(228/T) - 1]}{0{\cdot}6 + 0{\cdot}2\exp(-98/T) + \exp(228/T)}. \tag{19}$$

In order to obtain by numerical integration the vertical distribution of the optical depth shown in Fig. 3, it is useful to note that $\int_z^\infty n(\mathrm{O})\,\mathrm{d}z \simeq n(\mathrm{O})H(\mathrm{O})$ in an isothermal atmosphere; $H(\mathrm{O})$ is the atomic oxygen partial pressure scale height. Above 200 km, the optical depth is less than 10^{-2} for thermopause temperatures between 750 and 2000°K and for atomic oxygen concentrations adopted here. Figure 3 also shows a maximum optical depth between 3 and 4 for the atomic oxygen concentrations adopted in the lower thermosphere. It must be added that, if the time variations of the atomic oxygen distribution are important below 80 km, the optical depth is not strongly affected, since the main contribution comes from heights above 80 km.

5. FREQUENCY INTEGRATED INTENSITY AND MEAN VERTICAL FLUX

The specific intensity I_ν results from the integration of Equation (13b) after determining the boundary conditions.

At the upper boundary, a possible 63 μ source could be the Sun, since the solar brightness temperature at 63 μ should be around 4500°K (Nagel, 1968). With such a value and a mean dilution factor of $5{\cdot}4 \times 10^{-6}$, the specific intensity at 63 μ at the top of the Earth's atmosphere is $1{\cdot}6 \times 10^{-13}$ erg cm^{-2} sec^{-1} ster.$^{-1}$ Hz^{-1}. But at a height of 200 km, this specific intensity corresponds to the frequency integrated intensity ranging from $3{\cdot}8 \times 10^{-5}$ to $6{\cdot}2 \times 10^{-5}$ erg cm^{-2} sec^{-1} ster.$^{-1}$ for thermopause temperatures of 750 and 2000°K, respectively. Since the solar values are always negligible compared with the integrated intensities due to the ambient atomic oxygen below 200 km, it is assumed therefore that there is no incident radiation at the upper boundary where $\tau = 0$. But, at the lower boundary $\tau = \tau_0$, an ascending radiation $B(T_E)$ at 63 μ is assumed. With no absorption between the ground level and any altitude corresponding to $\tau = \tau_0$, $B(T_E)$ would be the specific intensity at 63 μ of a black body with a ground temperature T_E. But, since water

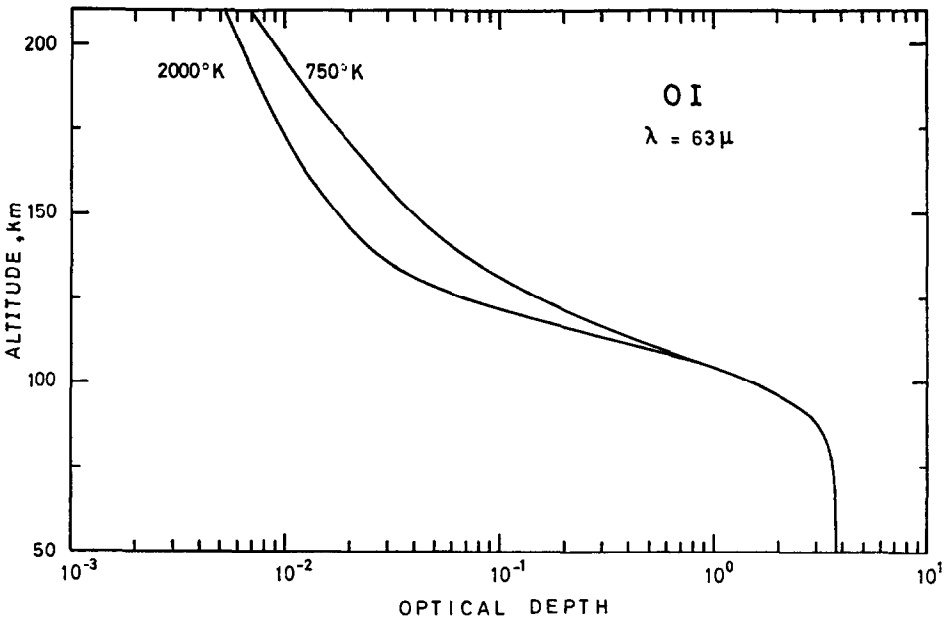

FIG 3. VERTICAL DISTRIBUTION OF THE OPTICAL DEPTH AT 63μ FOR THERMOPAUSE TEMPERATURES OF 750 AND 2000°K.

vapor has numerous rotational lines in this spectral region (Randall *et al.*, 1937) it may be assumed that the specific intensity at the lower boundary corresponds to a black body emission with a tropopause temperature, for example 190 or 216°K, for comparison with Craig and Gille (1969). The upward specific intensity at the lower boundary can then be written

$$B(T_E) = 1{\cdot}58 \times 10^{-9}[\exp(228/T_E) - 1]^{-1}. \tag{20}$$

For $T_E = 216$°K and $T_E = 190$°K, expression (20) gives $B(216°K) = 8{\cdot}4 \times 10^{-10}$ and $B(190°K) = 6{\cdot}8 \times 10^{-10}$ erg cm^{-2} sec^{-1} ster.$^{-1}$ Hz^{-1}, respectively.

Integration of Equation (13b) gives then the frequency integrated intensity for the *ascending* radiation $I_+(\tau, u)$, u being positive,

$$I_+(\tau, u) = \Delta\nu \left\{ \int_\tau^{\tau_0} \exp\left[\frac{\tau - t}{u}\right] B(T) \frac{\mathrm{d}t}{u} + B(T_E) \exp\left[\frac{\tau - \tau_0}{u}\right] \right\}. \tag{21}$$

In Equation (21), $\Delta\nu$ is given by (16); the spectral distribution $B(T)$ is similar to (20) and is a function of the optical depth, because the kinetic temperature T depends on the altitude. If the emission at the lower boundary is not exactly given by (20) only the second term in (21) must be corrected. Without any emission at the upper boundary, the frequency integrated intensity $I_-(\tau, u)$ for the *descending* radiation, u being negative, is given by

$$I_-(\tau, u) = -\Delta\nu \left\{ \int_0^{\tau} \exp\left[\frac{\tau - t}{u}\right] B(T) \frac{\mathrm{d}t}{u} \right. . \tag{22}$$

The values of I_+ and I_- obtained by numerical integration of (21) and (22) are measured in erg cm^{-2} sec^{-1} ster^{-1}. The variation with height is obtained by means of the optical depth derivative (19).

Figure 4 shows distributions of I_+ and I_-, obtained for $u = \pm 1$, i.e. vertical conditions. First of all, above 120 km, the highest intensities correspond to the highest thermopause temperature and the ascending intensity is stronger than the descending intensity I_- which has been measured by Feldman and McNutt (1969) and by Houck and Harwit (1969). Above 120 km, I_+ is not affected by the presence of an emission $B(T_E)$ at the lower boundary. The values between 10^{-2} and 4×10^{-2} erg cm^{-2} sec^{-1} ster.$^{-1}$ are entirely due to the

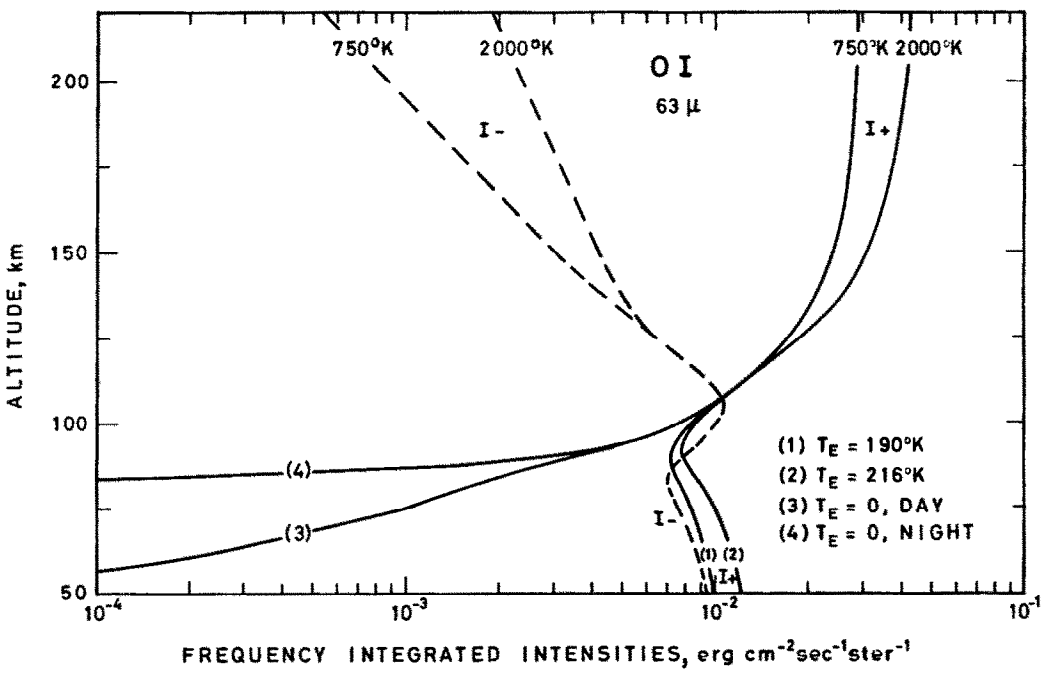

FIG. 4. VERTICAL DISTRIBUTION OF THE FREQUENCY INTEGRATED INTENSITIES I_- AND I_+ FOR THERMOPAUSE TEMPERATURES OF 750 AND 2000°K.
The curves labelled (1), (2), (3) and (4) correspond to different conditions at the lower boundary.

emission of the ambient oxygen. Below 120 km, the physical situation becomes more complex. The minimum in I_- is due to the temperature minimum at the mesopause (85 km). The vertical distributions of I_+ are presented both taking into account and neglecting the lower boundary emission; they are shown in Fig. 4 by curves (1), (2), (3) and (4), respectively. In the latter case, the night-time atomic oxygen distribution below 90 km causes I_+ to decrease sharply (curve 4), while for an overhead Sun, corresponding to photochemical equilibrium conditions, the decrease is less pronounced. If lower boundary emissions corresponding to black bodies at 190 and 216°K are introduced, one obtains the curves labelled (1) and (2) below 90 km, which correspond to $9{\cdot}6 \times 10^{-3}$ and to $1{\cdot}2 \times 10^{-2}$ erg cm^{-2} sec^{-1} ster.$^{-1}$ at 50 km altitude, respectively. Finally, it must be pointed out that the descending intensity I_- is practically not affected in the lower thermosphere and in the mesosphere by the change from daytime to night-time conditions. Numerical values of

I_+ and I_- (MRayleigh) are given in Tables 4 and 5. When a lower boundary emission is involved, the intensity I_+ does not change between day and night in the mesosphere, for practical purposes.

TABLE 4. FREQUENCY INTEGRATED INTENSITIES (MRayleigh) IN THE THERMOSPHERE FOR THERMOPAUSE TEMPERATURES OF 750 AND 2000°K

z (km)	I_-		I_+	
	$T = 750$°K	$T = 2000$°K	$T = 750$°K	$T = 2000$°K
120	2·9	2·9	6·1	6·1
150	1·2	1·7	9·7	13·0
200	0·35	0·93	12·0	17·0
250	0·11	0·55	12·0	18·0

TABLE 5. FREQUENCY INTEGRATED INTENSITIES (MRayleigh) IN THE MESOSPHERE AND LOWER THERMOSPHERE

z (km)	I_-	I_+			
	Day and night	$T_E = 0$; night	$T_E = 0$; day	$T_E = 190$°K	$T_E = 216$°K
50	3·6	—	0·03	3·8	4·7
60	3·5	—	0·08	3·7	4·6
70	3·2	—	0·24	3·4	4·2
80	2·9	—	0·63	3·1	3·7
90	3·2	1·1	1·6	2·8	3·1
100	4·1	2·9	3·0	3·4	3·5
110	4·0	4·5	4·5	4·7	4·7

As the frequency-integrated intensities I_+ and I_- depend on the direction of the radiation, it is possible to compute a *mean ascending flux* F_+ and a *mean descending flux* F. In order to get F_+, it is necessary to integrate I_+ over one hemisphere, u varying from 1 to 0. The result of this integration is:

$$F_+(\tau) = 2\pi\Delta\nu \left\{ \int_\tau^{\tau_0} B(T)E_2(t - \tau)\,\mathrm{d}t + B(T_E)E_3(\tau_0 - \tau) \right. \tag{23}$$

where the exponential integral $E_n(x)$ is defined by

$$E_n(x) = \int_0^1 \exp\,(-x/u)u^{n-2}\,\mathrm{d}u. \tag{24}$$

The second term in (23) represents the contribution from the lower boundary emission. For a 2000°K thermopause temperature, $F_+(\tau)$ reaches values of the order of 0·2 erg cm^{-2} sec^{-1} above 200 km, whereas for 750°K, $F_+(\tau)$ is of the order of 0·11 erg cm^{-2} sec^{-1}.

When u varies from 0 to -1, one obtains the mean descending flux F_- in the form

$$F_-(\tau) = -2\pi\Delta\nu \int_0^\tau B(T)E_2(\tau - t)\,\mathrm{d}t. \tag{25}$$

The maximum value of $F_-(\tau)$ is reached around 110 km and is of the order of 0·04 erg cm^{-2} sec^{-1}.

It is also interesting to define a *mean net flux* $F(\tau)$ by

$$F(\tau) = F_+(\tau) + F_-(\tau). \tag{26}$$

This quantity is used in the computation of the volume emission rate in next section. As F_+ and F_- have opposite signs, the mean net flux F can reach negative values. F is always positive above 120 km, but at lower heights, the sign of F is directly related to the relative importance of I_+ and I_- (see Fig. 4). If the lower boundary emission is taken into account, F is negative below 110 km, but again becomes positive around the mesopause. Due to this behaviour, an infrared heating zone is introduced which is discussed in detail in the next section.

6. VOLUME EMISSION RATE

The frequency integrated emission described in the preceding section is the parameter to be deduced from an observational determination. In the thermal balance of the upper atmosphere, it is necessary however to know the rate energy loss or gain. The divergence of the heat flow transported by conduction as well as the heat production by ultraviolet absorption and the heat loss by infrared radiation are simultaneously involved in the heat conduction equation.

The volume emission rate (erg cm^{-3} sec^{-1}) of atomic oxygen is in fact given by the divergence of the mean net flux F defined in the preceding section. As a function of altitude z, the volume emission rate $L(z)$ is written as follows

$$L(z) = \frac{dF}{d\tau}\frac{d\tau}{dz} \tag{27}$$

where $d\tau/dz$ is given by (19).

By using the expressions (4), (23) and (24), one obtains

$$L(z) = L(63\,\mu)[1 - X] \tag{28}$$

where

$$X = \left[0{\cdot}5 \exp(228/T) - 0{\cdot}5\right]\left[\int_0^{\tau_0} \frac{E_1(|t-\tau|)\,dt}{\exp(228/T) - 1} + \frac{E_2(\tau_0 - \tau)}{\exp(228/T_E) - 1}\right]. \tag{29}$$

In (28), $L(63\,\mu)$ is the infrared loss (4) corresponding to an optically thin atmosphere, and in (29) $|t - \tau|$ represents the absolute value of $t - \tau$; the term containing the second order exponential integral E_2 in (29) is due to the lower boundary emission. Stewart (1968) obtained an expression similar to (28) and the result of Craig and Gille (1969) can be found by performing an integration by parts in (29). It is also possible to show that the factor X is equal to

$$X = J_\nu(z)/B(T) \tag{30}$$

where J_ν is the mean value of the specific intensity $I_\nu = I/\Delta\nu$ integrated over a sphere and $B(T)$ is a Planck's function at $63\,\mu$ characterized by the kinetic temperature T of the atmosphere.

Figure 5 shows the volume emission rate computed for different conditions. The numerical technique is briefly discussed in the Appendix. If the factor X is neglected, the distribution corresponding to an optically thin atmosphere is obtained. In this case, the infrared emission always corresponds to a heat loss, which could reach values as high as $1{\cdot}5 \times 10^{-7}$ erg cm^{-3} sec^{-1} in the neighbourhood of 100 km. Such a value is comparable and even greater than the heat production by ultraviolet absorption in the vicinity of 120

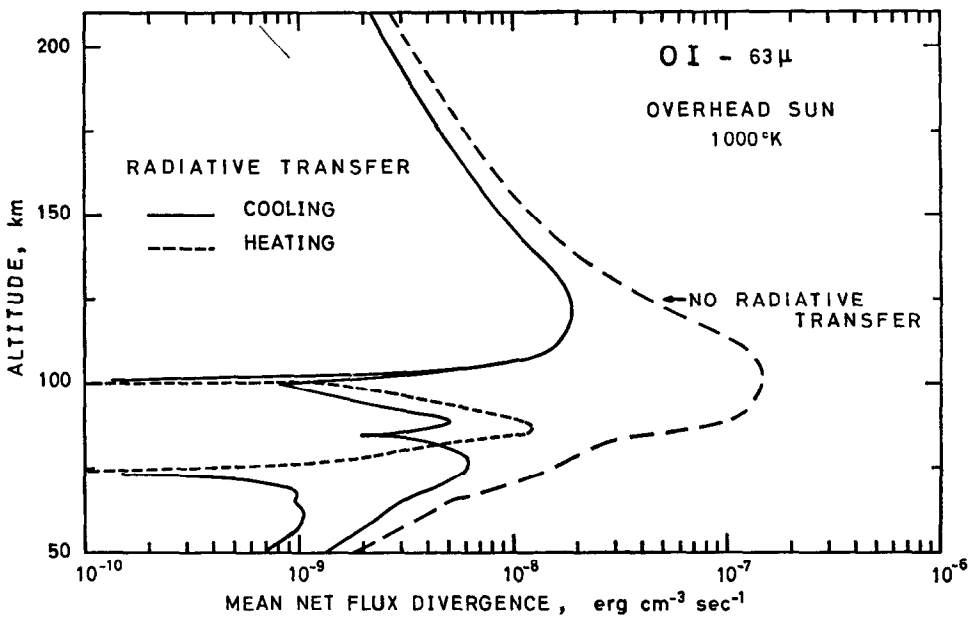

FIG. 5. VERTICAL DISTRIBUTION OF THE VOLUME EMISSION RATE FOR A 1000°K THERMOPAUSE TEMPERATURE.
Comparison with the optically thin case.

km for an overhead Sun. The atomic oxygen infrared emission is therefore an important factor in the development of atmosphere models between 100 and 150 km. When the radiative transfer is introduced, the heat loss around 120 km is of the order of 2×10^{-8} erg cm^{-3} sec^{-1}, i.e. a value still comparable to the heat deposited by ultraviolet absorption at those heights.

Around 100 km, $L(z)$ changes its sign or goes through an extremum. It corresponds to the level where the optical depth τ is practically half of the optical depth τ_0 of the lower boundary. This property can be mathematically proved for a constant temperature. If the lower boundary emission is neglected, $L(z)$ increases below 100 km and reaches a maximum and a second extremum occurs at the mesopause. On the other hand the introduction of a lower boundary emission leads to a sign change for $L(z)$ and a heating zone appears in the vicinity of the mesopause. The existence of this infrared heating zone has also been found by Stewart (1968), by Craig and Gille (1969), and by Shved and Nerushev (1969). For daytime conditions (see Fig. 5) a small cooling, previously unnoticed, appears below this heating zone. Since atomic oxygen disappears very quickly below 80 km after sunset, the daytime cooling shown in Fig. 5 disappears in the mesosphere at night.

In order to show the exact effect of radiative transfer, the reduction factor $1\text{-}X$, indicating the departure from an optically thin layer, is presented in Fig. 6. It varies from 0·79 ($T = 750$°K) to 0·90 ($T = 2000$°K) above 200 km, corresponding to a decrease of the infrared loss by 10–20 per cent, compared to the case of an optically thin layer. The reduction factor increases when the optical depth increases. Below 100 km, the reduction factor is also given without lower boundary emission. In this case, the infrared emission always corresponds to a cooling. Figure 6 also shows the effect of the minimum in the mesopause temperature.

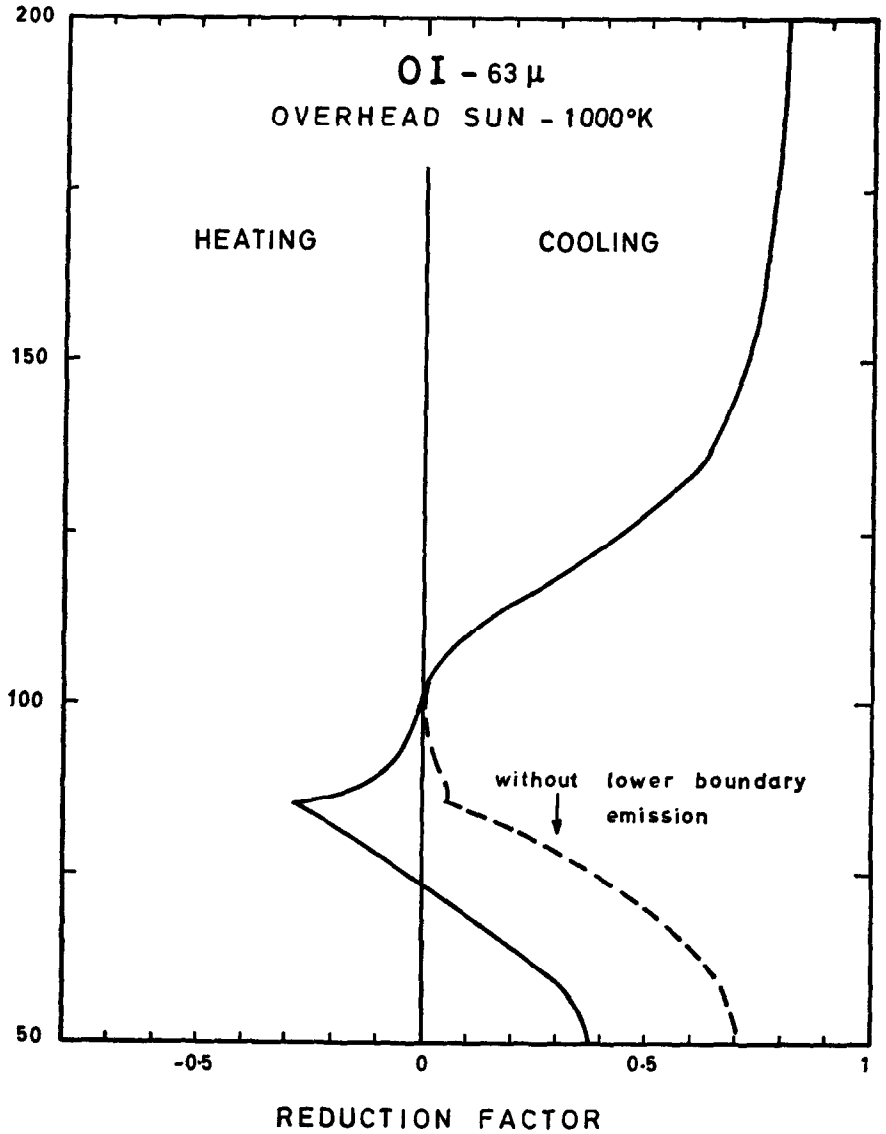

FIG. 6. VERTICAL DISTRIBUTION OF THE REDUCTION FACTOR 1-X FOR A 1000°K THERMOPAUSE TEMPERATURE.
Negative values correspond to a heating.

7. EFFECT OF THE ATOMIC OXYGEN CONCENTRATION

The rocket observation (Feldman and McNutt, 1969) of the 63 μ emission was made on 28 March 1968. An estimate of the night-time temperature during the flight yields a value of the order of 1000°K.

The intensity (erg cm^{-2} sec^{-1} $column^{-1}$) for an optically thin layer (Equation (4)) is represented in Fig. 7 by dashed lines for two models with the same temperature distribution, but with atomic oxygen concentrations differing by a factor of 2. When radiative transfer

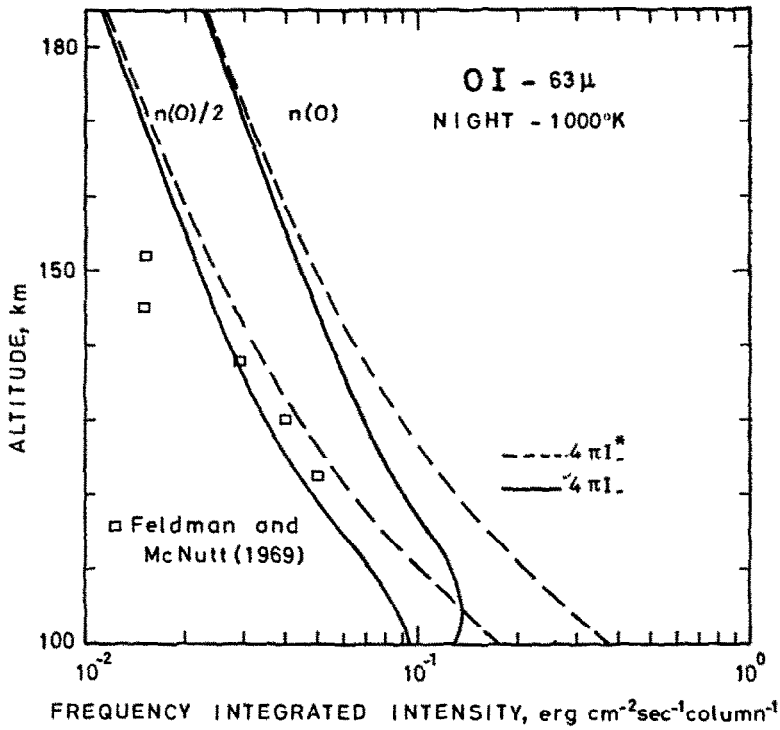

FIG. 7. COMPARISON BETWEEN EXPERIMENTAL AND THEORETICAL FREQUENCY INTEGRATED INTENSITY FOR A MODEL CORRESPONDING TO A THERMOPAUSE TEMPERATURE AT 1000°K. Effect of a decrease of the atomic oxygen concentration.

is taken into account, the full lines show that there is no direct proportionality to a reduction in the atomic oxygen concentration, especially when the optical depth becomes high. The observational results obtained by Feldman and McNutt (1969) seem to indicate (Fig. 7) that, on 28 March 1968, the atomic oxygen concentration is less than 10^{11} cm^{-3} at 120 km but is greater than 5×10^{10} cm^{-3}.

In Fig. 7, the curves labelled $n(O)/2$ can also be interpreted as corresponding to a vertical intensity, while the curves labelled $n(O)$ correspond to an observational zenith angle of 60°.

In the 100–200 km region, infrared measurements of the 63 μ line can yield valuable informations on the atomic oxygen concentration, since the frequency integrated intensities as well as the volume emission rates are rather sensitive to a change in the atomic oxygen number density. Table 6 shows how some parameters previously discussed may vary if the atomic oxygen concentration is decreased by a factor two.

TABLE 6. FREQUENCY INTEGRATED INTENSITIES, VOLUME EMISSION RATE AND REDUCTION FACTOR

	$z = 100$ km, $T = 209$°K		$z = 120$ km, $T = 324$°K	
	$n(O) = 3{\cdot}2 \times 10^{11}$ cm^{-3}	$n(O) = 1{\cdot}6 \times 10^{11}$ cm^{-3}	$n(O) = 10^{11}$ cm^{-3}	$n(O) = 5 \times 10^{10}$ cm^{-3}
I_+(erg cm^{-2} sec^{-1} ster.$^{-1}$)	$8{\cdot}77 \times 10^{-3}$	$9{\cdot}02 \times 10^{-3}$	$1{\cdot}54 \times 10^{-2}$	$1{\cdot}37 \times 10^{-2}$
I_-(erg cm^{-2} sec^{-1} ster.$^{-1}$)	$1{\cdot}03 \times 10^{-2}$	$7{\cdot}50 \times 10^{-3}$	$7{\cdot}26 \times 10^{-3}$	$3{\cdot}75 \times 10^{-3}$
L(erg cm^{-3} sec^{-1})	$-1{\cdot}43 \times 10^{-9}$	$3{\cdot}34 \times 10^{-9}$	$1{\cdot}82 \times 10^{-8}$	$1{\cdot}34 \times 10^{-8}$
$1 - X$	$-9{\cdot}9 \times 10^{-3}$	$4{\cdot}6 \times 10^{-2}$	$3{\cdot}0 \times 10^{-1}$	$4{\cdot}4 \times 10^{-1}$

8. CONCLUSION

The experimental data (Feldman and McNutt, 1969) for the 63 μ line of atomic oxygen available at the present time concern the frequency integrated intensity I_-. It is, however, interesting to measure also the upward intensity I_+, which is more intense than I_- above 120 km and which is due entirely to the emission of the ambient oxygen. On the other hand, the slope of I_+ is always less than the one of I_- above 120 km. Finally, it is to be noted that radiative transfer should be used for the interpretation of observational data below 150 km.

When the mean net flux is computed, one can see that the infrared loss is principally towards interplanetary space for altitudes above 100 km. At heights above 100 km, the infrared loss is important in the heat conduction equation. Between 100 km and 150 km, radiative transfer must be taken into account, because otherwise the infrared loss would be overestimated by more than one order of magnitude. In order to compute the volume emission rate when temperature changes with time it is necessary to solve the complete heat conduction equation in the thermosphere.

The effect of the heating layer near the mesopause should be added to the effect due to carbon dioxide in a study of the thermal balance in the mesosphere.

Finally, it is clear that measurements of the 63 μ OI line offer the possibility of determining the atomic oxygen distribution in the lower thermosphere which is not yet precisely known.

REFERENCES

ABRAMOWITZ, M. and STEGUN, I. A. (Editors) (1964). *Handbook of Mathematical Functions with Formulas, Graphs, and Mathematical Tables*, p. 1046. National Bureau of Standards, Applied Mathematics Series, 55, Washington, D.C.

BATES, D. R. (1951). The temperature of the upper atmosphere. *Proc. phys. Soc.* **64B**, 805.

CHANDRASEKHAR, S. (1960). *Radiative Transfer*, 393 pp. Dover, New York.

COLEGROVE, D. F., JOHNSON, F. S. and HANSON, W. B. (1966). Atmospheric composition in the lower thermosphere. *J. geophys. Res.* **71**, 2227.

CRAIG, R. A. and GILLE, J. C. (1969). Cooling of the thermosphere by atomic oxygen. *J. atmos. Sci.* **26**, 205.

FELDMAN, P. D. and MCNUTT, D. P. (1969). Far infrared nightglow emission from atomic oxygen. *J. geophys. Res.* **74**, 479.

HALL, L. A., CHAGNON, C. W. and HINTEREGGER, H. E. (1967). Daytime variations in the composition of the upper atmosphere. *J. geophys. Res.* **72**, 3425.

HINTEREGGER, H. E. and HALL, L. A. (1969). Thermospheric densities and temperatures from EUV absorption measurements by OSO-III. *Space Research IX*, p. 519. North-Holland, Amsterdam.

HOUCK, J. R. and HARWIT, M. (1969). Far infrared nightglow emission from atomic oxygen. *Science* **164**, 1271.

KRANKOWSKY, D., KASPRZAK, W. T. and NIER, A. O. (1968) Mass spectrometric studies of the composition of the lower thermosphere during Summer 1967. *J. geophys. Res.* **73**, 7291.

MAUERSBERGER, K., MULLER, D., OFFERMANN, D. and VON ZAHN, U. (1968). A mass spectrometric determination of the neutral constituents in the lower thermosphere above Sardinia. *J. geophys. Res.* **73**, 1071.

MITCHELL, A. C. G. and ZEMANSKY, M. W. (1961). *Resonance Radiation and Excited Atoms*, p. 338. Cambridge University Press, New York.

MÜNCH, G. (1962). The intensity of forbidden emission lines. *Astrophys. J.* **136**, 823.

NAGEL, M. R. (1968). Problems and programs on the use of the submillimeter waves in space, p. 47. *NASA Spec. Publ.* No. 182 Washington D.C.

NICOLET, M., BANKS, P. M. and KOCKARTS, G. (1970). Introduction to the study of aeronomy. *Handb. Phys* Bd. 49/4. Springer, Berlin (In press).

RANDALL, H. M., DENNISON, D. M., GINSBURG, N. and WEBER, L. R. (1937). The far infrared spectrum of water vapor. *Phys. Rev.* **52**, 160.

SHVED, G. M. and NERUSHEV, A. F. (1969). The thermal effect of radiative transfer in the atomic oxygen line near 63μ. *Fiz. Atmosf. Okeana, U.S.S.R.* **5**, 473.

STEWART, R. W. (1968). Radiative terms in the thermal conduction equation for planetary atmospheres. *J. atmos. Sci.* **25**, 744.

WIESE, W. L., SMITH, M. W. and GLENNON, B. M. (1966). Atomic transition probabilities. *Hydrogen Through Neon*, Vol. 1. p. 153. National Standard Reference Data System, Washington D.C.

APPENDIX

The integrals involved in the computation of the optical depth of the frequency integrated intensities and of the fluxes can be evaluated by applying a 5-point Bode rule (Abramowitz and Stegun, 1964).

However, the integrand appearing in the volume emission rate (28) and (29) is characterized by a singular point for $t = \tau$. It is actually necessary to evaluate

$$Y = \int_0^a f(x)E_1(x)\,dx \tag{A1}$$

$E_1(x)$ being the first exponential integral and $f(x)$ being a smooth function of x. Craig and Gille (1969) solved this difficulty by performing an analytical integration by parts before the numerical integration. This procedure leads to the numerical computation of $df(x)/dx$, which can present some difficulties.

For an integration step h, it is possible to write a general expression as follows:

$$\int_{x_0}^{x_0+h} f(x)E_1(x)\,dx = f(x_0)E_2(x_0) - f(x_0+h)E_2(x_0+h) + [E_3(x_0) - E_3(x_0+h)][f(x_0+h) - f(x_0)]/h + R \tag{A2}$$

where the absolute value of R is such that

$$|R| < (\tfrac{1}{8})f''(\xi)h^2[E_2(0) - E_2(h)] \tag{A3}$$

with

$$x_0 \leqslant \xi \leqslant x_0 + h.$$

The accuracy of an integration method based on expression (A2) is a little less than the trapezoidal rule. It is therefore suitable to split (A1) into two parts. First,

$$Y_1 = \int_h^a f(x)E_1(x)\,dx \tag{A4}$$

is evaluated with a five-point Bode rule. Second,

$$Y_2 = \int_0^h f(x)E_1(x)\,dx \tag{A5}$$

is evaluated by modifying expression (A2). It is possible to show that

$$\int_0^h f(x)E_1(x)\,dx \simeq 0{\cdot}5[f(h) + f(0)][1 - E_2(h)] + 0{\cdot}5h[f(h) - f(0)][-1/2 + h/6]. \tag{A6}$$

Integration steps of 1 km have been used in the computations and expression (A6) can give a contribution of the order of 25 per cent to the integral (A1).

Finally, the exponential integrals $E_1(x)$ and $E_2(x)$ have been computed with an accuracy of 8 digits.